PAPER

Check for updates

GNPS-guided discovery of xylacremolide C and D, evaluation of their putative biosynthetic origin and bioactivity studies of xylacremolide A and B†

Felix Schalk,‡[a] Janis Fricke, [iD] ‡[a] Soohyun Um,[a] Benjamin H. Conlon, [iD] [b] Hannah Maus, [iD] [c] Nils Jäger,[d] Thorsten Heinzel,[d] Tanja Schirmeister, [iD] [c] Michael Poulsen [iD] [b] and Christine Beemelmanns*[a]

Targeted HRMS[2]-GNPS-based metabolomic analysis of *Pseudoxylaria* sp. X187, a fungal antagonist of the fungus-growing termite symbiosis, resulted in the identification of two lipopeptidic congeners of xylacremolides, named xylacremolide C and D, which are built from D-phenylalanine, L-proline and an acetyl-CoA starter unit elongated by four malonyl-CoA derived ketide units. The putative *xya* gene cluster was identified from a draft genome generated by Illumina and PacBio sequencing and RNAseq studies. Biological activities of xylacremolide A and B were evaluated and revealed weak histone deacetylase inhibitory (HDACi) and antifungal activities, as well as moderate protease inhibition activity across a panel of nine human, viral and bacterial proteases.

Introduction

While most fungal species belonging to the genus *Xylaria* (Ascomycota: Xylariaceae) are of saprotrophic nature and globally abundant,[1,2] members of the subgenus *Pseudoxylaria* thrive predominantely on deteriorating comb material of fungus-cultivating termites that live in an obligate symbiosis with specialized fungal cultivars in the genus *Termitomyces* (Basidiomycotina).[3,4] Our recent studies focused on the relationship between the termite's fungal cultivar and the competitive and/or antagonistic behaviour of *Pseudoxylaria* to better understand their coevolutionary relationship.[5,6] Based on the metabolomic analysis of fungus–fungus co-cultures, we found that isolate *Pseudoxylaria* sp. X802 produces several biologically active small molecules including the antibacterial tetracyclic peptides pseudoxylallemycins and epoxy-cytochalasins.[7,8] Following up on this, we performed a high resolution tandem mass spectrometry (HRMS[2])-based analysis of guttation

droplets that appear on aging aerial hyphae of the isolate X187 (Fig. 1a).[9] Processing of the MS[2]-data using Global Natural Products Social Molecular Networking Analysis (GNPS)[10] revealed the production of four linear peptides called pseudoxylaramides A–D and two PKS-NRPS based hybrids named xylacremolides A and B.[11] The identified xylacremolides share similar structural features with acremolides[12] and FR235222,[13] a known histone deacetylase inhibitor, isolated from *Acremonium* spp. and saroclides from the mangrove-derived fungus *Sarocladium kiliense* HDN11-112.[14] Intrigued by the high abundance of xylacremolide A and B in guttation droplets of *Pseudoxylaria* sp. X187 (from now on named X187), and inspired by the findings that fungal PKS-based megaenzymes are often inherently promiscuous, we intensified our metabolomic and genomic analysis of X187. Here, we report for the first time on the characterization of two novel xylacremolide congeners named xylacremolide C and D, and on detailed bioactivity studies of xylacremolide A and B. *In silico* analysis of genomic and RNA sequencing data of X187 allowed us to propose a putative biosynthetic PKS-NRPS-based gene cluster of xylacremolides in *Pseudoxylaria* for the first time.

Results and discussion

Metabolomic analysis and isolation

HRMS[2]-based metabolomic analysis of guttation droplet of X187 and subsequent GNPS-based visualization of the acquired MS[2]-data was performed according to an established procedure (Fig. 1b and S1†).[11] GNPS-networks were screened for molecular ion peaks belonging to xylacremolide A and B and putative structural congeners that varied in chain length and oxidation

[a]*Chemical Biology of Microbe-Host Interactions, Leibniz Institute for Natural Product Research and Infection Biology, Hans Knöll Institute (HKI), Beutenbergstraße 11a, 07745 Jena, Germany. E-mail: Christine.beemelmanns@hki-jena.de*

[b]*Section for Ecology and Evolution, Department of Biology, University of Copenhagen, Universitetsparken 15, 2100 Copenhagen East, Denmark*

[c]*Institute of Pharmaceutical and Biomedical Sciences, Johannes Gutenberg University Mainz, Staudingerweg 5, 55128 Mainz, Germany*

[d]*Institute of Biochemistry and Biophysics at Center for Molecular Biomedicine (CMB), Department of Biochemistry, Friedrich Schiller University Jena, Hans-Knöll-Straße 2, 07745 Jena, Germany*

† Electronic supplementary information (ESI) available. See DOI: 10.1039/d1ra00997d
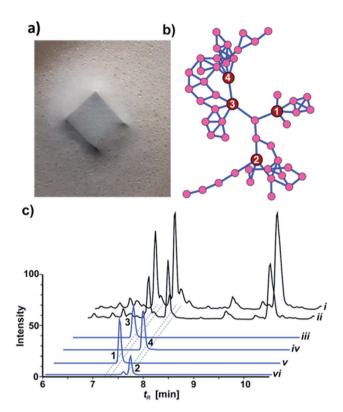
‡ Contributed equally.

Fig. 1 (a) *Pseudoxylaria* sp. X187 with guttation droplets on PDA; (b) GNPS network showing three distinct clades of substructures containing molecular ion peaks related to xylacremolides A (**3**), B (**4**), C (**1**) and D (**2**); (c) top to bottom: LC-MS chromatogram comparing TICs of crude culture extracts of X187 grown on PDA (i) or ISP2 medium (ii); XICs of compounds **1–4** (iii–vi), ±5 ppm range. Intensity (100%) was set to 4 × 10⁹ for (i)–(iv) and 4 × 10⁸ for (v) and (vi).

Fig. 2 (a) Structures of isolated xylacremolides C (**1**) and D (**2**); (b) representative COSY and HMBC correlation of xylacremolide C (**1**); (c) structures of previously isolated xylacremolides A (**3**) and B (**4**) from X187.

of the PKS moiety. The identified m/z subnetwork related to xylacremolide A and B (m/z 403.223 (**3**), m/z 417.238 (**4**)) contained a total of 50 connected nodes with molecular ion peaks that were partially assigned to congeners carrying additional methylene units ($\Delta m/z$ 14.016, $\Delta m/z$ 28.032) and derivatives with varying C_2H_4OH moieties ($\Delta m/z$ 45.057). The subcluster containing molecular ion peaks of **3** and **4** was connected by a single node (m/z 443.252) to two additional subclusters containing the molecular ion peaks m/z 461.263 and m/z 459.248, respectively. Subsequent dereplication of HRMS values using Antibase and Scifinder indicated that X187 might produce yet unreported xylacremolide congeners.[11]

We then evaluated the relative abundance of identified molecular ion peaks in culture extracts obtained from different growth conditions. Methanolic extracts were obtained from cultures grown on potato-dextrose-agar (PDA; samples taken after 18, 28 and 42 days) and ISP2 medium (samples taken after 18 and 42 days). Subsequent comparative HRMS-analysis of culture extracts revealed a very stable xylacremolide composition within all extracts with xylacremolide B as the main product, followed by non-methylated derivative xylacremolide A (Fig. 1c, S2 and Table S1†). Although the abundance of other molecular ion peaks belonging to putative new congeners was found to be about one order of magnitude lower compared to
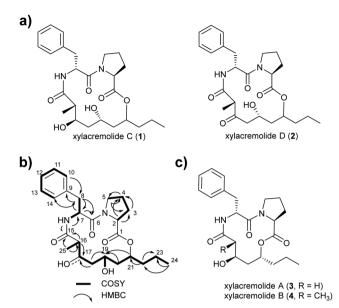
xylacremolide B, we pursued a MS-guided isolation of those molecular ions peaks (Fig. 1).

For this purpose X187 was grown on 30 plates (PDA, 26 °C) and mycelium-covered agar plates were extracted with methanol after 28 days. Culture extracts were subjected to MS-guided semi-preparative liquid chromatography yielding two new xylacremolide congeners, xylacremolide named C (**1**) and D (**2**) in analytical purity (Fig. 2 and S3†). The first isolated molecule (HR-ESI-MS m/z [M + H]⁺ calcd for $C_{25}H_{37}O_6N_2$ 461.2646, found 461.2644, Δ_{ppm} = −0.434) was structurally analyzed by comparative 1D (¹H and ¹³C) and 2D (HSQC, COSY, and HMBC) NMR spectroscopy (Tables 1, S2 and Fig. S6–S11†). On the basis of the molecular formula, nine degrees of unsaturation were conjectured. The ¹H NMR spectrum of **1** showed features of a peptidic compound bearing two α-proton signals [δ_H 4.85 and 4.25] and one NH signal [δ_H 8.46]. Also, three carbonyl carbon signals [δ_C 174.9, 171.9, and 169.8] and two α-carbon signals [δ_C 59.7 and 51.3] based on the HSQC and HMBC spectra supported that compound **1** is a peptide-derived compound (Table S1†). Comparative analysis of ¹H and 2D NMR data of **1** and revealed two amino acid residues including a proline (Pro) and a phenylalanine (Phe) and 3,5,7-trihydroxy-2-methyldecanoic acid (TMDA). The α-proton [H-2, δ_H 4.85] of Pro showed homonuclear correlations to H-3 [δ_H 2.02 and 1.79]. Additional ¹H–¹H correlations of H-3/H-4 [δ_H 1.80 and 1.45], H-4/H-5 [δ_H 3.79 and 3.37] and respective HMBC correlations from H-2 to C-3 [δ_C 29.5], H-3 to C-2 and C-4 [δ_C 59.7 and 24.9], and H-5 [δ_H 3.79, 3.72] to C-3 and C-4 supported the assumption of a ring structure (Fig. 2b).

Similarly, the α-proton [H-7, δ_H 4.85] of Phe revealed ¹H–¹H-COSY correlations to H-8 [δ_H 2.92 and 2.86] and the amide proton [δ_H 8.46]. The connectivities were supported by HMBC correlations from the α-proton H-7 to C-8 [δ_C 36.7], from the H-8

Table 1 Chemical shift values of compound **1** and **2** (600/125 MHz, DMSO-d_6)

Nr	**1** ^{13}C	^{1}H (J in Hz)	**2** ^{13}C	^{1}H (J in Hz)
1	171.9, s	—	174.6, s	—
2	59.7, d	4.26, dd (8.5, 2.5)	59.4, d	4.32, m
3	29.5, t	2.02, m	26.8, t	2.02, m
		1.79, m		1.79, m
4	24.9, t	1.80, m	24.3, t	1.80, m
		1.45, m		1.54, m
5	47.1, t	3.79, m	47.0, t	3.78, m
		3.37, m		3.43, m
6	169.8, s		167.1, s	
7	51.3, d	4.85, ddd (9.0, 7.5, 6.0)	51.4, d	4.94, ddd (9.0, 7.5, 6.0)
8	36.7, t	2.92, dd (13.5, 6.0)	36.0, t	2.92, dd (13.5, 6.0)
		2.86, dd (13.5, 9.0)		2.86, dd (13.5, 9.0)
9	138.2, s	—	138.1, s	—
10, 14	129.7, d	7.25, m	129.7, d	7.26, m
11, 13	128.4, d	7.25, m	128.4, d	7.26, m
12	126.7, d	7.17, m	126.7, d	7.18, m
NH		8.46, d (7.5)		8.96, d (7.5)
15	174.7, s		170.8, s	
16	42.1, d	2.61, m	51.5, d	3.58, q (6.5)
H_3-25	13.5, q	0.91, d (7.0)	13.6, q	0.91, d (6.5)
17	71.3, d	3.74, m	205.5, s	—
18	43.4, t	1.46, m	50.6, t	2.70, m
		1.37, m		2.18, m
19	64.4, d	3.77, m	63.2, d	4.28, m
20	41.7, t	1.83, m	33.9, t	1.85, m
		1.53, m		1.53, m
21	74.3, d	4.64, m	74.3, d	4.68, m
22	33.8, t	1.60, m	39.2, t	1.63, m
23	19.0, t	1.30, m	39.2, t	1.31, m
		1.23, m		1.28, m
24	13.5, q	0.89, dd (7.5, 7.5)	13.4, q	0.87, dd (7.5, 7.5)

to C-7 [δ_C 51.3], and from the NH proton to C-7; and the heteronuclear multi-bond correlations from H-8 to C-9 [δ_C 138.2] and C-10/C-14 [δ_C 129.7] of Phe. The benzene ring in the phenylalanine was determined by COSY and HMBC correlations between H-10/H-14 [δ_H 7.25] and C-12 [δ_C 126.7] and C-9, as well as from H-12 [δ_H 7.17] to C-10/C-14 [δ_C 129.7].

The trihydroxy-methyldecanoic acid (TMDA) was deduced by $^{1}H–^{1}H$ correlations from the methyl protons [H_3-25, δ_H 0.89] to the methine proton [H-16, δ_H 2.61] bearing three hydroxyl carbons [C-17, C-19, and C-21; δ_C 71.3, 64.4, and 74.3] and one methyl group [C-25, δ_C 13.5; δ_H 0.91] at C-16 [δ_C 42.1] supported by HMBC correlations. The connectivity of the two amino acid residues was confirmed with the NOESY correlation between H-5 of Pro and H-7 of Phe. The amide proton [δ_H 8.46] of Phe also showed HMBC correlation to the carbonyl carbon C-15 of TMDA. The nine degrees of unsaturation were in line with the weak HMBC correlation from the methine proton [C-21, δ_H 4.64] signal to the carbonyl carbon [C-1, δ_C 171.9] of Pro closing the 14-membered ring.

Due to its structural similarity to xylacremolide B (**4**), compound **1** was named xylacremolide C (**1**). Subsequently xylacremolide D (**2**) was also purified as an amorphous white powder and its molecular formula was deduced as $C_{25}H_{33}O_6N_2$ (HR-ESI-MS m/z [M + H]$^+$ calcd for $C_{25}H_{34}O_6N_2$ 459.2490, found 459.2485, Δ_{ppm} = −1.088). Comparative ^{1}H and 2D NMR analysis of **2** with those of **1** revealed a similar core structure with a carbonyl moiety at position at C-17 [δ_C 205.5], which was supported by HMBC correlations of H-16, 16-CH_3 and H-18 (Table S2 and Fig. S12–S15†).

Based on the assumption that xylacremolides share the same biosynthetic origin and the similar NMR chemical shift pattern, we deduced the identical stereochemical assignment for compound **1** and **2** as shown for xylacremolide B (**4**) by X-ray crystallography,[11] while the configuration at position C-21 remained unsolved.

Biosynthesis

To gain better insights into the enzymatic machinery responsible for the production of the xylacremolides, we thus sequenced X187 using Ilumina MiSeq and PacBio sequencing technology that yielded 499 contigs in a 39 Mbp draft genome assembly. We then set out to identify the putative biosynthetic pathway that was deduced to be of NRPS and PKS-based origin.[15–17] Mining of the obtained draft genome sequence using FungiSmash[18] revealed only one biosynthetic gene cluster (BGC) region, designated as the *xya* cluster (Fig. 3; GenBank accession number MW579544), that encodes for a highly-

Paper

reducing PKS (HRPKS) *xyaA* (KS-AT-DH-CMet-ER-KR), a bimodular nonribosomal peptide synthase (NRPS) *xyaB* (C_1-A_1-T_1-E_1-C_2-A_2-T_2-C_T), a major-facilitator superfamily (MFS) transporter *xyaC* and two short-chain dehydrogenases/reductases (SDR) *xyaD*/*xyaE*. Subsequent RNA-Seq analysis showed that all *xya* genes were transcribed under producing conditions. *In silico* analysis of the putative substrate preference of the A domains of

XyaB using NRPSPredictor2 [19] revealed a preference for D-Phe for A_1 and a hydrophobic amino acid with L-Pro being suggested by the closest neighbour prediction for A_2, which matches the structure of the xylacremolides. Additionally, the encoded proteins XyaA and XyaB showed high similarity (70% and 65% similar amino acid sequence) to the characterized ValA and ValB from *Aspergillus terreus* ATCC 20542, responsible for the
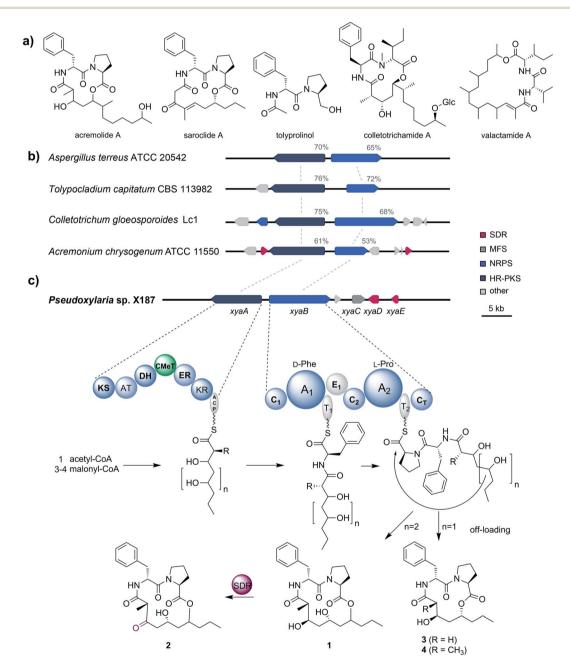

Fig. 3 (a) Structures of acremolide (*Acremonium* sp.), saroclide (*Sarocladium kiliense*), tolyprolinol (*Tolypocladium* sp. FKI-7981), colleto-trichamide (*Colletotrichum gloeosporioides* JS419), and valactamide (*Aspergillus terreus*). (b) Schematic representation of the *xya* BGC in *Pseudoxylaria* sp. X187 and comparison to homologues BGCs from *Aspergillus terreus* ATCC 20542, *Tolypocladium capitatum* CBS 113982, *Colletotrichum gloeosporioides* Lc1 and *Acremonium chrysogenum* ATCC 11550, which were identified using BLAST. Shown are genes coding for highly-reducing polyketide synthases (dark blue; HR-PKS), non-ribosomal peptide synthases (light blue; NRPS), short-chain dehydrogenases/reductases (red; SDR) and major facilitator superfamily transporters (dark grey; MFS). Non related genes are shown in light grey. Sequence similarities of the corresponding proteins of the homologues BGCs regarding XyaA/B are shown in percentages. (c) Proposed biosynthesis of the xylacremolides.

biosynthesis of the structurally related lipodepsipeptides valactamide A–H[20] (Fig. 3a). Furthermore, homologues BGCs have been identified *in silico* in other ascomycetes (Fig. 3b and Table S2†). Among them *Tolypocladium capitatum*, *Colletotrichum gloeosporioides* and *Acremonium chrysogenum*, produce tolyprolinol,[21] colletotrichamides[22] and acremolides,[12] which are all lipopeptides comprised of two amino acids and an aliphatic part pointing towards a similar biosynthetic origin (Fig. 3a). Although these three predicted BGCs have not yet been biochemically characterized, our findings support the assignment of the *xya* BGC and could set the stage for further biomolecular and biotechnological investigations.

The proposed biosynthetic assembly line for xylacremolides (Fig. 3c) is consistent with both the domain architectures of XyaA and XyaB and their molecular structure. Here, we propose that the KS domain of the iterative HRPKS XyaA incorporates an acetyl starter unit, followed by subsequent prolongation with either three or four malonyl-CoA derived ketide units. The first ketide is fully reduced to an alkane by the KR, DH and ER domains, whereas the following units are only partially reduced to the corresponding alcohols. Notably, the CMeT domain catalyzes the α-methylation of five membered polyketide chains, but can bypass this reaction in the four-membered products, which leads to the production of **3**. The C_1 domain of XyaB then catalyzes the amide bond formation of the tetra- and pentaketide chains with D-Phe, which was isomerized by the included E domain. Chain elongation is then catalyzed by the C_2 domain incorporating L-Pro, followed by macrolactonization by the C_T domain releasing the main products, which is typical for fungal NRPSes.[16–18] Subsequent tailoring oxidation reaction of the secondary alcohol (**1**) to the keto functionality of **2** could be catalyzed by either XyaD or XyaE; however incomplete reduction by XyaA cannot be excluded at this stage. Here, it is again noteworthy that congeners **1** and **2** are produced in a 2 : 1 ratio almost independently from the tested cultivation conditions (Table S1†).

Bioactivities of xylacremolide A and B

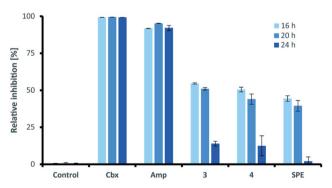Similar to their closest structural counterparts (acremolides), xylacremolides revealed so far no cytotoxic or antibacterial activities.[11] We then questioned which other cellular and/or ecological role xylacremolides might impose. A literature survey revealed that structurally related fungal metabolites trapoxin and FR235222 were previously investigated and found to be potent inhibitors of histone deacetylase (HDACi),[23,24] and are thus being investigated in cancer therapy, as well as in parasitic and inflammatory diseases. To test for HDACi activity, we selected the two most abundant xylacremolide derivatives, xylacremolides A and B, and found weak inhibitory activity of both compared to the positive controls valproic acid and trichostatin A (tested concentration range: 0.25–1.0 mM; Fig. S4†). We then tested both compounds for antifungal activity against *Aspergillus nidulans* RMS011 using a spore germination assay with carboxine and amphotericin B as positive controls (Fig. 4 and S5†).[25] Here, a moderate inhibitory effect of both compounds on spore germination was observed when spores were incubated for less than 20 h, while longer incubation times caused a significant decline in the inhibitory activity. Thus, it can be concluded that xylacremolides delays spore germination to moderate extent, but once *A. nidulans* is growing, it either tolerates or even detoxifies xylacremolides.

In light of the ecological origin of *Pseudoxylaria* sp. X187 (co-evolved antagonistic fungus of *Termitomyces*), it could be speculated at this point that the inhibitory activity of xylacremolides, while moderate, allows in combination with other metabolites an overall growth advantages and supports the successful out-competition of the fungal cultivar when colony homeostasis is disrupted.

In line with our long-term mission to identify pharmacologically relevant protease inhibitors, we tested the inhibitory activity of the two most abundant derivatives, xylacremolides A and B, on various pharmacologically important proteases using an established fluorescence-based assay (Table 2).[26–29] Both rhodesain (Rd), and cruzain, cysteine proteases belonging to the papain-family, play central roles in the life cycle of the parasitic protists *Trypanosoma brucei* (Human African Trypanosomiasis (HAT))[30] and *Trypanosoma cruzi* (Chagas-disease),[31] respectively. Three proteases were selected for their important functions in cancer cells (Cath L, Cath B, urokinase (uPA)).[32] Sortase A (SrtA)

Fig. 4 Antifungal activity assay of compound **3** and **4** and enriched SPE fraction of *Pseudoxylaria* sp. X187 crude extract (SPE) against *Aspergillus nidulans* RMS011. Carboxine (Cbx) and amphotericin B (Amp) served as positive controls. All substrates were tested at 1 μg mL^{-1}. The percentage of 0% inhibition is considered normal growth; while 100% are considered complete growth inhibition.

Table 2 Protease inhibitor activity screening of **3** and **4**

Protease	Compound **3**[a]/[%]	Compound **4**[a]/[%]
Cathepsin L	7.3 ± 3.3	11 ± 5.0
Cathepsin B	4.9 ± 1.4	n.i.
uPa	n.i.	n.i.
SrtA	3.8 ± 6.4	2.5 ± 4.2
Rhodesain	5.7 ± 5.2	15 ± 4.6
Cruzain	3.6 ± 2.3	3.8 ± 5.4
M^{pro} (SARS-CoV2)	n.i.	11 ± 9
PL^{pro} (SARS-CoV)	n.i.	11 ± 14
DENV2	n.i.	4.8 ± 4.8
ZIKV	0.7 ± 1.2	17 ± 3.4

[a] Inhibition at a compound concentration of 200 μM in DMSO as a percentage mean value ± standard deviation with $n = 3$. Inhibition rates below 0.5% are given as n.i. (no inhibition).

was selected as promising antibacterial target due to its protease and transpeptidase activity related to the formation of the peptidoglycan layer of *Staphylococcus aureus*.[33] For antiviral activity testing, we selected four proteases (ZIKV NS2B-NS3 protease,[34] DENV2-NS2B-NS3,[35] M[pro] (also known as 3C like protease and which is the main protease of the novel corona virus SARS-CoV2),[36] and PL[pro]).[37] Initial inhibitor screening was performed at compound concentrations of 200 μM in DMSO, which revealed mild inhibition of cruzain, cathepsin L, DENV2 NS2B-NS3, SARS-CoV(2) M[pro] and PL[pro], SrtA and moderate inhibition of rhodesain and ZIKV NS2B-NS3. Despite overall moderate activity, it was interesting to observe that methylated xylacremolide B showed in most cases higher inhibitory activities compared to non-methylated xylacremolide A.

Experimental

Compound identification based on GNPS analysis

Pseudoxylaria sp. X187-2 was grown on 30 potato-dextrose (PD) agar plaes (0.8 L of PDA, 2% agar, standard plates 16 mm × 92 mm, 20 mL per plate) for four weeks at room temperature. Mycelium-covered agar plates were cut into small pieces (0.5 cm × 0.5 cm), extracted twice with 300 mL MeOH, and methanolic extracts dried under vacuum. Crude extracts were subjected to UPLC-ESI-HRMS measurements (Dionex Ultimate 3000 system combined with a Q-Exactive Plus mass spectrometer equipped with an electrospray ion (ESI) source (Thermo Scientific)). The resulting HRMS[2] was subjected to MS[2] fragmentation based network analysis carried out on the global natural products social molecular networking platform (GNPS). The data was filtered by removing all MS/MS peaks within ±17 Da of the precursor m/z. MS/MS spectra were window filtered by choosing only the top 6 peaks in the ±50 Da window throughout the spectrum. The data was then clustered with MS-Cluster with a parent mass tolerance of 0.02 Da and a MS/MS fragment ion tolerance of 0.02 Da to create consensus spectra. Further, consensus spectra that contained less than 2 spectra were discarded. A network was then created where edges were filtered to have a cosine score above 0.7 and more than 6 matched peaks. Further, edges between two nodes were kept in the network if each of the nodes appeared in each other's respective top 5 most similar nodes. Finally, the maximum size of a molecular family was set to 50, and the lowest scoring edges were removed from molecular families until the molecular family size was below this threshold.

Analysis of production levels

Pseudoxylaria sp. X187-2 was cultivated on 30 PDA and 30 ISP2 agar plates (0.6 L, 2% agar, 16 × 92 mm plates, 20 mL per plate). Fungal plates were grown for up to six weeks at room temperature. Cultures were extracted with methanol and extracts of four biological replicates were combined and concentrated. The crude extract was re-dissolved in 20% MeOH (unless stated otherwise: ddH$_2$O was used as second solvent) and loaded on an activated and equilibrated SPE C18ec column (1 g, Macherey-Nagel). The SPE cartridge was washed with two column volumes 20% MeOH and one column volume 50% MeOH. Metabolites were eluted in fractions by stepwise elution from 60% to 100% MeOH (two column volumes each fraction). The resulting 60% and 80% MeOH SPE fractions were combined dried under reduced pressure and re-dissolved in MeOH to yield 50 μg mL^{-1}. Particles were removed by centrifugation for 15 min at 13.000 rpm and submitted for LC-MS based quantification. Compounds 1–4 were quantified based on integration of corresponding XICs (AUC, area under the curve, Δ5 ppm range) using the automatic peak detection feature in Xcalibur™. The AUC of xylacremolide A (3) was set to 100% and the abundance of the other derivatives was normalized based on their AUC relative to 3 in the same sample.

Large-scale cultivation

Pseudoxylaria sp. X187-2 was cultivated on 30 PDA 16 × 92 mm, 20 mL per plate, 2% agar) and plates incubated for four weeks at room temperature. Mycelium-covered agar plates were cut into small pieces and extracted twice with 600 mL MeOH. Extracts were filtered through filter paper, concentrated under reduced pressure, and enriched using C18 SPE cartridges as described before. Xylacremolides A–D eluted predominantly as a mixture within the 60% MeOH fraction with some residual elution in the 80% MeOH fraction from the SPE column. Fractions were concentrated under reduced pressure to yield a white-brown solid material which was subjected to further purification by semi-preparative HPLC until analytical compounds were obtained.

Structure elucidation

Xylacremolide C (1). White solid; $[\alpha]_D^{25}$ −0.18 (*c* 0.1 w/v%, MeOH); UV (acetonitrile), λ_{max} 201, 219 nm; IR (ATR) ν_{max} 3743, 3621, 3311, 2702, 2322, 1616, 1562 cm^{-1}; NMR spectral data, see Table S2;† HRMS (ESI) m/z [M + H]$^+$ calcd for C$_{25}$H$_{37}$O$_6$N$_2$ 461.2646, found 461.2644, Δ_{ppm} −0.434.

Xylacremolide D (2). White solid; $[\alpha]_D^{25}$ −1.63 (*c* 0.1 w/v%, MeOH); UV (acetonitrile), λ_{max} 201, 219 nm; IR (ATR) ν_{max} 3412, 3290, 2821, 2704, 2325, 2023, 1660 cm^{-1}; NMR spectral data, see Table S2;† HRMS (ESI) m/z [M + H]$^+$ calcd for C$_{25}$H$_{34}$O$_6$N$_2$ 459.2490, found 459.2485, Δ_{ppm} −1.088.

Genome sequencing and *in silico* analysis. DNA extractions for whole-genome sequencing were performed using a scaled-up CTAB extraction. Whole-genome sequencing was performed using a 150 bp paired-end shotgun (BGIseq) and long-read (PacBio sequel) sequencing by BGI (Hongkong). Sequencing results were checked for quality using FastQC version 0.11.8 (ref. 38) and MultiQC version 1.7.[39] Kmer depth was calculated using Jellyfish version 2.2.10 (ref. 40) and Kmer-based estimates of genome size, heterozygosity and repeat content generated using GenomeScope.[41] A hybrid *de novo* genome assembly, combining BGISeq and PacBio data, was performed using SPAdes version 3.13.0.[42] Gen models were predicted with Augustus.[43] Homologues gene clusters were identified using the protein–protein BLAST (blastp) function from the NCBI. RNA-Seq data was mapped against the identified

xya gene cluster and expression levels were calculated using Geneious Prime 2021.0.3 (Biomatters, Ltd.). Gene cluster region and RNA transcripts were uploaded to GenBank (NCBI).

Protease inhibition assays.[26–29] Compounds were dissolved in DMSO (20 mM). Fluorometric assays were performed at a concentration of 200 μM. The inhibitory effect of compounds was determined for the following enzymes: rhodesain, cruzain, cathepsin L, cathepsin B, SARS-CoV2 M[pro], SARS-CoV PL[pro], DENV2 NS2B-NS3, ZIKV NS2B-NS3, urokinase (uPA), sortase A (SrtA). Assay conditions were: 45 μL buffer, 1.25 μL enzyme in buffer, 2.5 μL compound in DMSO, 1.25 μL substrate in DMSO (total volume 50 μL). The increase of the fluorescence was recorded over a period of 10 min in intervals of 30 s (exception: SrtA 30 min). Inhibition was calculated from the slope of fluorescence increase in the presence of the compound in relation to the slope in the presence of DMSO.

Buffers and substrates. Rhodesain (50 mM Na-acetate pH 5.5, 5 mM EDTA, 200 mM NaCl, 5 mM DTT, 10 μM Z-Phe-Arg-AMC); cruzain (50 mM Na-acetate pH 5.5, 5 mM EDTA, 200 mM NaCl, 5 mM DTT, 5 μM Z-Phe-Arg-AMC); cathepsin L (50 mM Tris pH 6.5, 5 mM EDTA, 200 mM NaCl, 2 mM DTT, 6.25 μM Z-Phe-Arg-AMC); cathepsin B (50 mM Tris pH 6.5, 5 mM EDTA, 200 mM NaCl, 2 mM DTT, 100 μM Z-Phe-Arg-AMC); SARS-CoV2 M[pro] (20 mM Tris pH 7.5, 0.1 mM EDTA, 200 mM NaCl, 1 mM DTT, 50 μM Dabcyl-KTSAVLQS GFRKME-Edans); SARS-CoV PL[pro] (20 mM Tris pH 7.5, 0.1 mM EDTA, 200 mM NaCl, 1 mM DTT, 50 μM Z-Arg-Leu-Arg-Gly-Gly-AMC); DENV2 and ZIKV NS2B-NS3 (50 mM Tris pH 9.0, 20% glycerol, 1 mM Chaps, 100 μM Boc-Gly-Arg-Arg-AMC); urokinase (50 mM Tris pH 7.4, 50 mM NaCl, 0.5 mM EDTA, 240 μM Z-Gly-Gly-Arg-AMC), sortase A (5 mM Tris pH 7.5, 15 mM NaCl, 0.5 mM CaCl$_2$, 0.5 mM Gly$_4$, 25 μM Abz-LPETG-Dap(dnp)-OH).

Conclusions

Reinvestigation and intensified HRMS^2-GNPS-based metabolomic analysis of *Pseudoxylaria* sp. X187 resulted in the identification of two additional lipopeptidic congeners of xylacremolides, which we named xylacremolide C and D. While xylacremolide A and B are built from three malonyl-CoA derived ketide units, the newly identified congeners are built from four malonyl-CoA derived ketide units, which indicates towards a promiscuous PKS. Evaluation of possible biological activities revealed moderate to weak antifungal and HDACi activity, as well as moderate protease inhibition activities across a panel of nine human, viral and bacterial proteases. Although their single bioactivities alone are likely not responsible for the antagonistic behaviour of *Pseudoxylaria* sp. X187, the combined actions might allow for a considerable growth advantage.

Author contributions

Conflicts of interest

There are no conflicts to declare.

Acknowledgements

Notes and references

1 F. Song, S.-H. Wu, Y.-Z. Zhai, Q.-C. Xuan and T. Wang, *Chem. Biodiversity*, 2014, **11**, 673–694.

2 S. E. Helaly, B. Thongbai and M. Stadler, *Nat. Prod. Rep.*, 2018, **35**, 992–1014.

3 M. Poulsen, H. Hu, C. Li, Z. Chen, L. Xu, S. Otani, S. Nygaard, T. Nobre, S. Klaubauf, P. M. Schindler, F. Hauser, H. Pan, Z. Yang, A. S. M. Sonnenberg, Z. Wilhelm De Beer, Y. Zhang, M. J. Wingfield, C. J. P. Grimmelikhuijzen, R. P. De Vries, J. Korb, D. K. Aanen, J. Wang, J. J. Boomsma and G. Zhang, *Proc. Natl. Acad. Sci. U. S. A.*, 2014, **111**, 14500–14505.

4 S. Otani, V. L. Challinor, N. B. Kreuzenbeck, S. Kildgaard, S. Krath Christensen, L. L. M. Larsen, D. K. Aanen, S. A. Rasmussen, C. Beemelmanns and M. Poulsen, *Sci. Rep.*, 2019, **9**, 1–10.

5 A. A. Visser, V. I. D. Ros, Z. W. De Beer, A. J. M. Debets, E. Hartog, T. W. Kuyper, T. Læssøe, B. Slippers and D. K. Aanen, *Mol. Ecol.*, 2009, **18**, 553–567.

6 A. A. Visser, P. W. Kooij, A. J. M. Debets, T. W. Kuyper and D. K. Aanen, *Fungal Ecol.*, 2011, **4**, 322–332.

7 H. Guo, N. B. Kreuzenbeck, S. Otani, M. Garcia-Altares, H. M. Dahse, C. Weigel, D. K. Aanen, C. Hertweck, M. Poulsen and C. Beemelmanns, *Org. Lett.*, 2016, **18**, 3338–3341.

8 H. Guo, A. Schmidt, P. Stephan, L. Raguž, D. Braga, M. Kaiser, H. M. Dahse, C. Weigel, G. Lackner and C. Beemelmanns, *ChemBioChem*, 2018, **19**, 2307–2311.

9 M. Gareis and C. Gottschalk, *Mycotoxin Res.*, 2014, **30**, 151–159.

10 M. Wang, J. J. Carver, V. V. Phelan, L. M. Sanchez, N. Garg, Y. Peng, D. D. Nguyen, J. Watrous, C. A. Kapono, T. Luzzatto-Knaan, C. Porto, A. Bouslimani, A. V. Melnik,

M. J. Meehan, W. T. Liu, M. Crüsemann, P. D. Boudreau, E. Esquenazi, M. Sandoval-Calderón, R. D. Kersten, L. A. Pace, R. A. Quinn, K. R. Duncan, C. C. Hsu, D. J. Floros, R. G. Gavilan, K. Kleigrewe, T. Northen, R. J. Dutton, D. Parrot, E. E. Carlson, B. Aigle, C. F. Michelsen, L. Jelsbak, C. Sohlenkamp, P. Pevzner, A. Edlund, J. McLean, J. Piel, B. T. Murphy, L. Gerwick, C. C. Liaw, Y. L. Yang, H. U. Humpf, M. Maansson, R. A. Keyzers, A. C. Sims, A. R. Johnson, A. M. Sidebottom, B. E. Sedio, A. Klitgaard, C. B. Larson, C. A. P. Boya, D. Torres-Mendoza, D. J. Gonzalez, D. B. Silva, L. M. Marques, D. P. Demarque, E. Pociute, E. C. O'Neill, E. Briand, E. J. N. Helfrich, E. A. Granatosky, E. Glukhov, F. Ryffel, H. Houson, H. Mohimani, J. J. Kharbush, Y. Zeng, J. A. Vorholt, K. L. Kurita, P. Charusanti, K. L. McPhail, K. F. Nielsen, L. Vuong, M. Elfeki, M. F. Traxler, N. Engene, N. Koyama, O. B. Vining, R. Baric, R. R. Silva, S. J. Mascuch, S. Tomasi, S. Jenkins, V. Macherla, T. Hoffman, V. Agarwal, P. G. Williams, J. Dai, R. Neupane, J. Gurr, A. M. C. Rodríguez, A. Lamsa, C. Zhang, K. Dorrestein, B. M. Duggan, J. Almaliti, P. M. Allard, P. Phapale, L. F. Nothias, T. Alexandrov, M. Litaudon, J. L. Wolfender, J. E. Kyle, T. O. Metz, T. Peryea, D. T. Nguyen, D. VanLeer, P. Shinn, A. Jadhav, R. Müller, K. M. Waters, W. Shi, X. Liu, L. Zhang, R. Knight, P. R. Jensen, B. Palsson, K. Pogliano, R. G. Linington, M. Gutiérrez, N. P. Lopes, W. H. Gerwick, B. S. Moore, P. C. Dorrestein and N. Bandeira, *Nat. Biotechnol.*, 2016, **34**, 828–837.

11 F. Schalk, S. Um, H. Guo, N. B. Kreuzenbeck, H. Görls, Z. W. de Beer and C. Beemelmanns, *ChemBioChem*, 2020, **21**, 2991–2996.

12 R. Ratnayake, L. J. Fremlin, E. Lacey, J. H. Gill and R. J. Capon, *J. Nat. Prod.*, 2008, **71**, 403–408.

13 H. Mori, F. Abe, S. Furukawa, S. Furukawa, F. Sakai, M. Hino and T. Fujii, *J. Antibiot.*, 2003, **56**, 80–86.

14 W. Guo, S. Wang, N. Li, F. Li, T. Zhu, Q. Gu, P. Guo and D. Li, *J. Nat. Prod.*, 2018, **81**, 1050–1054.

15 A. Vassaux, L. Meunier, M. Vandenbol, D. Baurain, P. Fickers, P. Jacques and V. Leclère, *Biotechnol. Adv.*, 2019, **37**, 107449.

16 A. S. Brown, M. J. Calcott, J. G. Owen and D. F. Ackerley, *Nat. Prod. Rep.*, 2018, **35**, 1210–1228.

17 D. Yu, F. Xu, S. Zhang and J. Zhan, *Nat. Commun.*, 2017, **8**, 1–11.

18 K. Blin, S. Shaw, K. Steinke, R. Villebro, N. Ziemert, S. Y. Lee, M. H. Medema and T. Weber, *Nucleic Acids Res.*, 2019, **47**, W81–W87.

19 M. Röttig, M. H. Medema, K. Blin, T. Weber, C. Rausch and O. Kohlbacher, *Nucleic Acids Res.*, 2011, **39**, 362–367.

20 K. D. Clevenger, J. W. Bok, R. Ye, G. P. Miley, M. H. Verdan, T. Velk, C. Chen, K. Yang, M. T. Robey, P. Gao, M. Lamprecht, P. M. Thomas, M. N. Islam, J. M. Palmer, C. C. Wu, N. P. Keller and N. L. Kelleher, *Nat. Chem. Biol.*, 2017, **13**, 895–901.

21 W. Fukasawa, N. Mori, M. Iwatsuki, R. Hokari, A. Ishiyama, M. Nakajima, T. Ouchi, K. Nonaka, H. Kojima, H. Matsuo, Ō. Satoshi and K. Shiomi, *J. Antibiot.*, 2018, 2–4.

22 S. Bang, C. Lee, S. Kim, J. H. Song, K. S. Kang, S. T. Deyrup, S. J. Nam, X. Xia and S. H. Shim, *J. Org. Chem.*, 2019, **84**, 10999–11006.

23 R. Randino, I. Moronese, E. Cini, V. Bizzarro, M. Persico, M. Grimaldi, M. Scrima, A. M. D'Ursi, E. Novellino, E. Sobarzo-Sanchez, L. Rastrelli, C. Fattorusso, A. Petrella, M. Rodriquez and M. Taddei, *Curr. Top. Med. Chem.*, 2017, **17**, 441–459.

24 N. J. Porter and D. W. Christianson, *ACS Chem. Biol.*, 2017, **12**, 2281–2286.

25 M. C. Monteiro, M. De La Cruz, J. Cantizani, C. Moreno, J. R. Tormo, E. Mellado, J. R. De Lucas, F. Asensio, V. Valiante, A. A. Brakhage, J. P. Latgé, O. Genilloud and F. Vicente, *J. Biomol. Screening*, 2012, **17**, 542–549.

26 P. Klein, F. Barthels, P. Johe, A. Wagner, S. Tenzer, U. Distler, T. A. Le, P. Schmid, V. Engel, B. Engels, U. A. Hellmich, T. Opatz and T. Schirmeister, *Molecules*, 2020, **25**, 2064.

27 F. Barthels, G. Marincola, T. Marciniak, M. Konhäuser, S. Hammerschmidt, J. Bierlmeier, U. Distler, P. R. Wich, S. Tenzer, D. Schwarzer, W. Ziebuhr and T. Schirmeister, *ChemMedChem*, 2020, **15**, 839–850.

28 A. Welker, C. Kersten, C. Müller, R. Madhugiri, C. Zimmer, P. Müller, R. Zimmermann, S. Hammerschmidt, H. Maus, J. Ziebuhr, C. Sotriffer and T. Schirmeister, *ChemMedChem*, 2021, **16**, 340–354.

29 B. Millies, F. von Hammerstein, A. Gellert, S. Hammerschmidt, F. Barthels, U. Göppel, M. Immerheiser, F. Elgner, N. Jung, M. Basic, C. Kersten, W. Kiefer, J. Bodem, E. Hildt, M. Windbergs, U. A. Hellmich and T. Schirmeister, *J. Med. Chem.*, 2019, **62**(24), 11359–11382.

30 D. Cullen and M. Mocerino, *Curr. Med. Chem.*, 2017, **24**, 701–717.

31 P. S. Doyle, Y. M. Zhou, I. Hsieh, D. C. Greenbaum, J. H. McKerrow and J. C. Engel, *PLoS Pathog.*, 2011, 7, 1–11.

32 M. J. Duffy, P. M. McGowan, N. Harbeck, C. Thomssen and M. Schmitt, *Breast Cancer Res.*, 2014, **16**, 1–10.

33 S. K. Mazmanian, G. Liu, E. R. Jensen, E. Lenoy and O. Schneewind, *Proc. Natl. Acad. Sci. U. S. A.*, 2000, **97**, 5510–5515.

34 W. W. Phoo, Y. Li, Z. Zhang, M. Y. Lee, Y. R. Loh, Y. B. Tan, E. Y. Ng, J. Lescar, C. Kang and D. Luo, *Nat. Commun.*, 2016, 7, 1–8.

35 X. Yao, S. Guo, W. Wu, J. Wang, S. Wu, S. He, Y. Wan, K. S. Nandakumar, X. Chen, N. Sun, Q. Zhu and S. Liu, *J. Pharmacol. Sci.*, 2018, **138**, 247–256.

36 Z. Jin, X. Du, Y. Xu, Y. Deng, M. Liu, Y. Zhao, B. Zhang, X. Li, L. Zhang, C. Peng, Y. Duan, J. Yu, L. Wang, K. Yang, F. Liu, R. Jiang, X. Yang, T. You, X. Liu, X. Yang, F. Bai, H. Liu, X. Liu, L. W. Guddat, W. Xu, G. Xiao, C. Qin, Z. Shi, H. Jiang, Z. Rao and H. Yang, *Nature*, 2020, **582**, 289–293.

37 M. Kandeel, Y. Kitade, M. Fayez, K. N. Venugopala and A. Ibrahim, *J. Med. Virol.*, 2021, **93**, 1581–1588.

38 S. W. Wingett and S. Andrews, *F1000Research*, 2018, 7, 1–13.

39 P. Ewels, M. Magnusson, S. Lundin and M. Käller, *Bioinformatics*, 2016, **32**, 3047–3048.

40 G. Marçais and C. Kingsford, *Bioinformatics*, 2011, **27**, 764–770.

41 G. W. Vurture, F. J. Sedlazeck, M. Nattestad, C. J. Underwood, H. Fang, J. Gurtowski and M. C. Schatz, *Bioinformatics*, 2017, **33**, 2202–2204.

42 A. Bankevich, S. Nurk, D. Antipov, A. A. Gurevich, M. Dvorkin, A. S. Kulikov, V. M. Lesin, S. I. Nikolenko, S. Pham, A. D. Prjibelski, A. V. Pyshkin, A. V. Sirotkin, N. Vyahhi, G. Tesler, M. A. Alekseyev and P. A. Pevzner, *J. Comput. Biol.*, 2012, **19**, 455–477.

43 M. Stanke, R. Steinkamp, S. Waack and B. Morgenstern, *Nucleic Acids Res.*, 2004, **32**, 309–312.